JOURNAL OF EXPERIMENTAL AND THEORETICAL PHYSICS, 2024, Vol. 166, No. 3 (9), pp. 405–416

STATISTICAL, NONLINEAR, AND SOFT MATTER PHYSICS

IONOSPHERIC PLASMA-DUST CLOUDS: INFLUENCE OF RAYLEIGH-TAYLOR INSTABILITY

© 2024 Yu. S. Reznichenko [a, b, *], A. Yu. Dubinsky [a], S. I. Popel [a, **]

[a] Space Research Institute of Russian Academy of Sciences, IKI RAS 117997, Moscow, Russia
[b] Moscow Institute of Physics and Technology (National Research University), MIPT 141701, Dolgoprudny, Moscow region, Russia

*e-mail: reznichenko.yus@phystech.edu
**e-mail: popel@iki.rssi.ru

Received February 09, 2024
Revised April 07, 2024
Accepted April 26, 2024

Abstract. Noctilucent clouds (NLC) and polar mesosphere summer echoes (PMSE) of the Earth's ionosphere, observed at altitudes of about 80-95 km, are considered. A self-consistent model describing a possible formation mechanism of such clouds is presented. It is shown that, unlike the ionosphere of Mars, the influence of such factors as dust particle interaction with adhering water condensate molecules and viscous Knudsen friction strength decrease in the nucleation zone decreases on the Earth. The characteristic sizes and charges of the dust particles of the cloud predicted by the model are calculated. It is shown that an important factor, affects the formation of dusty plasma clouds of the Earth's mesosphere, is the Rayleigh–Taylor instability. The effect of the instability leads to the fact that there is an upper limit of the size of the dust particles in the cloud.

Keywords: *Earth, ionosphere, NLC, PMSE, dust particles, Rayleigh–Taylor instability*

DOI: DOI: 10.31857/S004445102409e128

1. INTRODUCTION

Dusty plasma is an ionized gas that contains, in addition to electrons, ions, and neutral atoms and molecules, solid matter particles and/or liquid droplets, typically of micron or submicron sizes. Dust particles and droplets that are part of dusty plasma can either form spontaneously within it or be introduced from outside [1]. Due to interaction with electrons and ions, as well as under the influence of solar radiation, dust particles quickly acquire an electric charge, which significantly complicates plasma dynamics: new types of waves and instabilities appear (in particular, the presence of dust acoustic mode, generation of nonlinear waves due to the development of dust acoustic instability, see [2, 3]), self-organization processes can lead to the formation of droplets, clouds, various structures, plasma-dust crystals [1, 4] etc.

In nature, dust plasma is very widespread; it is found in the lunar exosphere [5, 6], in cometary tails [7], in planetary ionospheres and magnetospheres [8–10], in interstellar space [11]. Moreover, in the Solar system, it is practically impossible to find an area filled with plasma without dust impurities (the only exception, perhaps, is the Sun itself and the zone directly around it) [1]. Therefore, it is not surprising that with the development of a sufficient number of various methods for describing dust plasma [12–16], more and more attention has been paid to studies of planetary ionospheres. In addition to general theoretical interest, such studies can have purely applied significance, as they are useful for atmospheric physics, ecology, and geophysics [9]. On Earth, for example, one cannot exclude the relationship between plasma-dust ionospheric phenomena and various types of climatic changes, in particular, with global warming processes [10].

Typical examples of dust layers of plasma origin are terrestrial noctilucent clouds (NLC) and polar mesosphere summer echoes (PMSE) [17-19]. These atmospheric phenomena are registered in the summer at similar altitudes, and the appearances of noctilucent clouds and polar mesosphere summer echoes strongly correlate with each other. All this gives reason to assume that the mechanism of formation and conditions for the appearance of NLC and PMSE are fundamentally the same. The characteristic size of NLC particles is several hundred nanometers, with the maximum size not exceeding one micrometer. Noctilucent cloud particles mainly consist of ice, however, the presence of impurities, including metallic ones, is possible [17]. The appearance of noctilucent clouds, as mentioned above, is limited to the summer season and occurs at mesospheric altitudes (about 80–85 km) in high and middle latitudes. A characteristic feature of noctilucent clouds is the possibility of observing them at sunset with the naked eye.

PMSE, unlike NLC, cannot be detected by any known optical methods; their detection is indirect: polar mesosphere summer echoes appear as strong radar echoes at radars operating in the frequency range from 50 to 1000 MHz [18]. These clouds are located higher than NLC, at altitudes from 85 to 95 km. The characteristic size of charged PMSE particles is most likely nanometers [19] or tens of nanometers [20].

In the last two decades, moreover, the presence of dust clouds on Mars has been proven. For instance, the SPICAM infrared spectrometer (installed on the Mars Express spacecraft [21]) detected clouds at altitudes of about 100 km, consisting of particles with a characteristic size of about 100 nm. In March 2021, the Mars Science Laboratory Curiosity sent images to Earth of similar clouds located at altitudes higher than 60 km [22]. The photography was conducted at sunset, when sunlight illuminated the surface of dust particles and highlighted the clouds against the dark sky (cf. what is known about Earth's noctilucent clouds). At lower altitudes (about 80 km above the planet's surface), the Mars Express mission using the OMEGA spectrometer discovered clouds consisting of micron-sized particles [23]. Clouds were also detected directly above the planet's surface and at altitudes of about 4 km [24], where thin dust layers consisting of frozen water ice or carbon dioxide particles were observed at night [25].

As noted above, some models (see, for example, [8–10, 26–28]) describing ionospheric dust clouds use methods developed for describing dusty plasma. These models have shown their applicability both on Earth and on Mars, providing good agreement with currently available experimental data. Initially, the object of study was NLC and PMSE of Earth's ionosphere, and subsequently, the model developed for Earth was adapted for dust clouds on Mars. This article proposes the development of a dust cloud model in Earth's atmosphere, proposed in [8–10], taking into account recent developments. Special attention is paid to studying the influence of the Rayleigh–Taylor instability on the formation of mesospheric plasma-dust structures.

2. CONDITIONS IN THE SUMMER POLAR MESOSPHERE

Plasma-dust mesospheric clouds are observed in the altitude range where a temperature anomaly is detected during the summer season and, as a result, the saturated water vapor pressure sharply decreases, leading to intensive growth of dust nuclei due to rapid condensation of atmospheric water vapor.

Dust nuclei in Earth's ionosphere are particles with a characteristic size of several nanometers. The sources of such particles are micrometeorite bombardment of the planet, volcanic eruptions, and forest fires. Micrometeorites entering the planet's atmosphere burn up at altitudes of 80–120 km with subsequent condensation of meteoric matter [29], while volcanic ash and soot particles rise from the lower atmospheric layers. Due to this, the concentration of nuclei strongly depends on the season and current micrometeorite activity. Usually, the average concentration value is in the range of 10–1000 cm^{-1}. Note that information about the composition and size distribution of such particles is provided only by rocket flying past experiments [30], as the detection of such particles by known optical methods is unfeasible. Therefore, the specified numerical data can only reproduce model representations of the dust component in Earth's mesosphere [29].

Under normal conditions, dust particles do not have a fundamental impact on ionospheric plasma dynamics. The situation, however, completely changes when gaseous substances present in the atmosphere become supersaturated. In

supersaturated vapors, dust particles actively grow and, upon reaching a certain size at a particular moment, begin to determine the ionization properties of the planetary ionosphere in their localization area [9]. Since particle growth is accompanied by interaction with the surrounding ionospheric plasma, particles quickly acquire an electric charge, which subsequently affects their growth. On Earth, this occurs at altitudes of about 80–95 km in the summer polar mesosphere. Here, the decrease in ambient air temperature to 150 K and below leads to the supersaturation of water vapor present in Earth's ionosphere (see, for example, [19]).

Figure 1 illustrates the conditions of Earth's summer polar mesosphere, important from the perspective of dust cloud physics. It shows altitude profiles of neutral gas temperature, saturated water vapor pressure, and actual (partial) water vapor pressure. The conditions for particle growth (nucleation) are met in the altitude range of about km, where water vapor is supersaturated. Note that it is in this altitude range where noctilucent clouds and polar mesosphere summer echoes are observed.

From the perspective of water vapor thermodynamics, the considered region of Earth's atmosphere can be divided into three characteristic parts: middle part with highly supersaturated water vapor and two peripheral regions of unsaturated vapor. From the perspective of dust particle dynamics, the upper region of unsaturated vapor can be called the zone of sedimentation with constant mass, the middle one the condensation zone, and the lower one the sublimation zone. In the condensation region, ionospheric dust nuclei grow due to desublimation of vapors H_2O, which makes possible the formation of a layered structure of the dust cloud [8, 9, 10, 26]. In the sublimation zone, previously condensed water vapor evaporates from the surface of dust particles, ultimately leading to the disappearance of the dust cloud, whose lifetime is thus determined by the sedimentation time of microparticles in the middle zone.

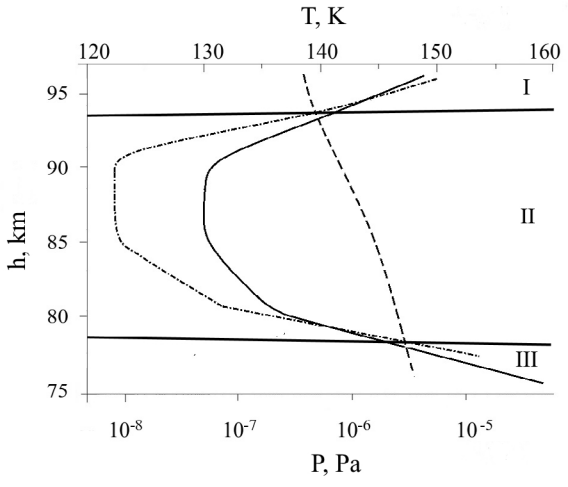

Fig. 1. Qualitative altitude profiles of air temperature (solid curve), partial pressure of water vapor (dashed curve), and saturated water vapor pressure (dash-dotted curve). Water vapor is supersaturated in the altitude range of 77–94 km. From the perspective of dust microparticle dynamics, the considered region of Earth's atmosphere can be divided into zones of sedimentation with constant mass (I), condensation (II), and sublimation (III)

Calculation of saturated water vapor concentration $n^S_{H_2O}$ above the particle surface is carried out in a standard way [31]. For this purpose, the thermodynamic potential of the system F, consisting of a dust particle with H_2O, molecules condensing on its surface, and the adjacent layer of gas of these molecules, is introduced. Since dust particles are charged and, furthermore, along with neutral molecules are surrounded by ions and electrons screening the dust particle field, it is necessary to take into account electrostatic interaction. Thus, the dependencies $n^S_{H_2O}$ on size a and charge $q_d = Z_d e$ of dust particles ($-e$ — electron charge), which is also a function of size of the particle, are taken into account. The thermodynamic potential of the system F has the form

$$\Phi = m_d(\tilde{f}_d + Pv_d) + m_g(\tilde{f}_g + Pv_g) + \\ + \mathsf{s}S + \Upsilon_E, \qquad (1)$$

where P — pressure, $\tilde{f}_d(v_d,T)$ — specific free energy of the dust particle, $\tilde{f}_g(v_g,T)$ is the specific free energy of the gas, $v_{d(g)}$ is the specific volume of the dust particle (gas), T is temperature, $m_{d(g)}$ is mass of dust particle (gas), s is surface tension coefficient of the particle substance, S is surface area of the dust particle. As for the electrostatic energy Υ_E, it consists of the electric field energy within the dust particle (index “in”) and in the remaining space (index “out”):

$$\Upsilon_E = \int_{in} \frac{eE^2}{8\pi} dV + \int_{out} \frac{E^2}{8\pi} dV. \qquad (2)$$

Here ε is the dielectric permittivity of the dust particle substance, E is the electric field, V is the volume.

The equation relating the value of pressure P_S of saturated H_2O vapors above a particle of size a, having a surface charge q_d, and the P_0 value of pressure of saturated H_2O vapors above a flat surface, is derived based on the analysis of extrema of expression (1) assuming spherical symmetry of the dust particle, constancy of value ε, and screening of the dust particle's electric field according to the Yukawa dependence. However, the influence of the dust particle charge on the condensation process is not very significant, therefore a simplified model presented in [9] can be used. The concentration value $n^S_{H_2O}$ is determined from P_S using the well-known ideal gas relation:

$$n^S_{H_2O} = \frac{P_S}{kT}.$$

Particle growth due to desublimation of supersaturated vapors is accompanied by their charging. A distinctive feature of the ionosphere at the considered altitudes is its complex composition (electrons, positive and negative ions are present). All positive ions can be conditionally divided into two groups. The first group includes simple (or primary) ions of nitrogen N_2^+, oxygen O_2^+ and nitrogen monoxide NO^+. The formation of primary ions occurs under solar radiation and as a result of electron impact ionization. The second group includes cluster (or proton-hydrated) ions of the type $H^+(H_2O)_n$ (where n is the degree of hydration, typically, $n \gtrsim 10$), which are converted from primary ions through a chain of charge exchange reactions [32]. The fundamental influence on the proportion of different types of positive ions in the mesosphere is exerted by the temperature of the surrounding neutral component T_n. which are converted from primary ions through a chain of charge exchange reactions [32]. The fundamental influence on the proportion of different types of positive ions in the mesosphere is exerted by the temperature of the surrounding neutral component 160 K, cluster ions with hydration parameter $n \ldots 10$ do not form, as the destruction of such ions during collisions with neutrals occurs much more effectively than their formation process from simple ions. As a result, there is a predominance of cluster ions with low hydration degree and primary ions. Note that the electron-ion recombination coefficient α_{rec} strongly depends on the type of ions: light simple ions have an effective recombination coefficient $\alpha_{rec} \sim 10^{-7}$ cm^{-3}s^{-1}, while cluster ions have $\alpha_{rec} \sim 10^{-5}$ cm^{-3}s^{-1}.

The presence of negative ions in the ionosphere is also possible [33], however, in our case, their presence is insignificant since, for example, the characteristic concentration of the most common ions O_2^- turns out to be equal to $N_{O_2^-} \approx 0.1$–1 cm^{-3} (see [9]), which is significantly lower than the characteristic concentrations of positive ions and electrons at the studied altitudes:

$$n_e \gg n_i \gg (q_e / \alpha_{rec})^{1/2} \gg 10^2 - 10^4 \text{cm}^{-3}.$$

Note that the consideration presented in the article takes into account a somewhat simplified model of the ionic composition of ionospheric plasma. Further improvement of the model involves using a more detailed ionic composition (see, for example, [34,35]).

The charging of microparticles occurs due to the recombination of electrons and ions on its surface, which, in turn, leads to a significant decrease in the concentration of the charged component of the ionosphere in the region of polar mesospheric clouds [9]. Another factor leading to the charging of microparticles can be the influence of solar radiation [8, 9]. The ionization of a dust particle due to the and is determined by the photoeffect is characterized by the rate q_{photo} and is determined by the solar radiation flux $F(\lambda)$ [8]:

$$q_{photo} \gg \frac{\pi a^2 \beta}{hc} \int_0^{\lambda^*} \lambda F(\lambda) d\lambda,$$

where λ^* is the maximum photon wavelength leading to the photoeffect (determined by the minimum energy of light quanta), β is the probability of the photoelectric effect. Typical values β usually lie within 10^{-4}–10^{-2}, and, as a rule, $\beta < 10^{-3}$ [9].

The minimum energy of light quanta $2\pi hc / \lambda^*$, leading to the photoeffect, is determined by the work function W of the dust particle material and its charge:

$$2\pi hc / \lambda^* = W - e^2 Z_d / a.$$

In this case, we can ignore the dependence of the photoelectron current on the dust particle charge

size, since the photon energy $2\pi\hbar c / \lambda^*$ is on the order of several eV, and the order of the equilibrium potential of the microparticle equals $\hbar$

$$e^2 |Z_d| / a \sim kT_e \simeq 0.01eV \ll 2\pi\hbar c / \lambda^*,$$

see [9], while $T_e / e \gg T_n / e$, where $T_n \gg 0.03$ eV is the temperature of the neutral ionospheric gas. Thus, we can consider that the maximum photon wavelength leading to the photoeffect is determined only by the work function of the dust particle material.

he influence of the photoeffect can be significant for relatively large particles; for nanoscale particles, the photoelectric effect's influence is not as substantial due to small absorption cross-section. Moreover, the high-energy part of the solar spectrum with ÿw...7.3 eV,which corresponds to $\lambda \approx 75$ nm, is intensively absorbed by the atmosphere at altitudes of $h \gg 100$ km (see [9]). The work function of ice W_{ice} is approximately 8.7 eV, therefore ice particles do not exhibit photoeffect and such particles carry a negative charge. However, if a particle contains metallic impurities, which is possible for particles of meteoric origin, there is a reduction in the work function W (for example, for iron $W \gg 4.6$ eV),and depending on its size, such a particle may carry a positive charge. The photoeffect in this case plays an important role in the ionization balance, as the ionization rate associated with the photoeffect becomes comparable to the ionization rate from natural sources:

$$q_{photo} \approx \pi a^2 \beta \Phi(\lambda^*) \sim 0.1 - 10\ cm^{-3} \cdot s^{-1} \sim q_e,$$

where

$$F(\lambda^*) = \int_0^{\lambda^*} F(\lambda) d\lambda$$

is cumulative radiation flux (see [9]).

3. THEORETICAL MODEL

When constructing a model of plasma-dust structures, the evolution of the dust particle distribution function $f_d(h,a,v,t)$ at height h is described using the kinetic equation

$$\frac{\partial f_d}{\partial t} + \frac{\partial f_d}{\partial a}\frac{da}{dt} + \frac{\partial f_d}{\partial h}\frac{dh}{dt} + \frac{\partial f_d}{\partial v}\frac{dv}{dt} = 0, \qquad (3)$$

$$\frac{da}{dt} = \frac{\alpha_{H_2O} m_{H_2O} v^{th}_{H_2O} \left(n_{H_2O} - n^S_{H_2O} \right)}{4\rho_d}, \qquad (4)$$

$$\frac{dv}{dt} = (mg - F_f + f)\frac{1}{m} = g - \frac{F_f}{m} + \frac{f}{m}, \qquad (5)$$

$$F_f = \pi\rho C_S a^2 F_d v, \qquad (6)$$

$$f = u\frac{dm}{dt}, \qquad (7)$$

$$\frac{dh}{dt} = -v, \qquad (8)$$

where α_{H_2O} — accommodation coefficient of water molecules upon collision with a dust particle (usually in highly supersaturated vapors $\alpha_{H_2O} \sim 1$), m and m_{H_2O} are the masses of the microparticle and water molecule respectively, n_{H_2O} ans $n^S_{H_2O}$ —actual and saturated concentrations of condensing water vapors, ρ and ρ_d are the densities of atmospheric gas and dust particle material, $v^{th}_{H_2O}$ and C_S are the thermal velocity of water molecules and sound speed in atmospheric gas, v is the dust particle velocity, $u = -v$ in the condensation zone and $u = 0$ in the sublimation zone, F_d — coefficient of order unity reflecting the influence of particle shape, g is the acceleration due to gravity. The second term in the left part (3) describes the growth of dust particles in the surrounding supersaturated water vapor, the fourth term describes sedimentation (rise) of the dust particle during interaction with neutrals (neutral drag) taking into account the term withc dm / dt in the equation of motion.

Since the speed of sound and the average thermal velocity are values of the same order, the contribution of each of the two braking factors (F_f / m and f/m) depends on the parameters of the ionosphere (density of condensing and/or resistance-creating gases). As shown in [36], under Martian atmospheric conditions, the settling regime of dust particles, despite the isotropic distribution of carbon dioxide, differs significantly for condensation and sublimation zones. Indeed, the dynamics of the “dust particle + gas” system in the condensation zone is described by equation

$$\frac{dP}{dt} = m\frac{dv}{dt} + v\frac{dm}{dt} = mg - F_f,$$

from which follows

$$m\frac{dv}{dt} = - v\frac{dm}{dt} + mg - F_f = mg - F_f + f,$$

where dm is the mass of condensing gas, P is the total momentum of the dust particle and gas. The concentrations of desublimating carbon dioxide are high, and the viscous friction force in this case is determined only by 5% of trace gases, therefore $F_f \ll f$ and the main braking factor is the interaction of the dust particle with condensate molecules adhering to it. In the sublimation zone, the term with f disappears, since in this case the evaporating carbon dioxide molecules and microparticle are at rest relative to each other. Physically, this means that molecules of evaporated CO_2 detached from the particle are decelerated not by particle acceleration but by transfer of kinetic energy to atmospheric molecules. Moreover, in the sublimation zone, all gas of the Martian atmosphere creates viscous friction force and, thus, the dynamics of gas and dust particle in this case is described by equation

$$\frac{dP}{dt} = m\frac{dv}{dt} = mg - F_f.$$

In the case of Earth's atmosphere, the density of condensing water vapor is negligible compared to the density of nitrogen and oxygen, which constitute the main mass of atmospheric gas. Thus, the concentration of neutral atmospheric gas at heights around 80 km is approximately $n_n \approx 5\times10^{14}$ cm^{-3}; water vapor pressure at this height is $P_{H_2O} \approx 10^{-6}$ Pa, which at $T \approx 130$ K gives $n_{H_2O} \approx P_{H_2O}/kT \approx 5\times10^{8}$ cm^{-3}. Therefore, firstly, the value of the relative correction of the Knudsen viscous friction force in the condensation zone is $n_{H_2O}/n_n \approx 5\cdot10^{8}/5\cdot10^{14} = 10^{-6} \ll 1$. Secondly, throughout the entire sedimentation time to Earth's surface, viscous friction makes the main contribution to microparticle deceleration. Indeed, since in the condensation zone $u \sim v$, $v^{th}_{H_2O} \sim$ CS, the ratio

$$f / F_f = u(dm/dt) / \pi C_S a^2 F_d v =$$

$$= u\alpha_{H_2O} m_{H_2O} v^{th}_{H_2O} \left(n_{H_2O} - n^S_{H_2O}\right) / \rho C_S F_d v \sim$$

$$\sim m_{H_2O}(n_{H_2O} - n^S_{H_2O}) / \rho \sim \rho_{H_2O} / \rho \ll 1.$$

Thus, compared to the Martian ionosphere, on Earth the influence of such factors as the interaction of dust particles with adhering water condensate molecules and the reduction of Knudsen viscous friction force in the nucleation region decreases.

It should also be noted that in the mesosphere it becomes possible to neglect the coagulation of dust particles during their collisions with each other [9]. The characteristic time τ_{coag} such a process significantly exceeds all other significant characteristic times:

$$\tau_{coag} \sim (n_d v \pi a^2)^{-1} .. 10^6 s.$$

Furthermore, it becomes possible to neglect the Brownian motion of particles. Indeed, the characteristic magnitude of particle displacement can be estimated using the formula

$$< x^2 >= 2kTB\tau = \frac{2kT\tau}{\pi C_S a^2},$$

where $B = 1/(\pi C_S a^2)$ is the particle mobility in a rarefied gas medium. At environmental temperature values T ~ 100 K, particle size a ~ 20–100 nm, sedimentation time τ ~ 1–10 h, typical for noctilucent clouds, the diffusion drift turns out to be ~ 0.01–10 m which is less than of the drop height.

The description of dust particles' influence on the dynamics of the charged ionosphere component is conducted using a system of equations consisting of four continuity equations [8. 91] and is written in local approximation (the use of local approximation is justified since in Earth's ionosphere the transport of dust particles occurs significantly faster than their charging). This system has the form

$$\frac{\partial n_e}{\partial t} = q_e - \alpha^s_{rec} n_e n_i^s - \alpha^c_{rec} n_e n_i^c + L^e_{photo} - L^e_{dust}, \tag{9}$$

$$\frac{\partial n_i^s}{\partial t} = q_e - \alpha^s_{rec} n_e n_i^s - \beta_c n_i^s - L^s_{dust}, \tag{10}$$

$$\frac{\partial n_i^c}{\partial t} = \beta_c n_i^s - \alpha^c_{rec} n_e n_i^c - L^c_{dust}, \tag{11}$$

$$\frac{\partial Z_d}{\partial t} = q_{photo} + \nu_s + \nu_c - \nu_e, \tag{12}$$

where n_e, n_i^s, n_i^c are the concentrations of electrons, primary and cluster positive ions respectively.

Here, the terms L^j_{dust} ($j = e, s, c$) describe the recombination of charged particles of ionospheric plasma (electrons, primary and proton-hydrated ions) on dust particles, taking into account the distribution dn_d of microparticles by size,

$$n_d = \int f_d \, dv da,$$

where

$$L^j_{dust} = \int \nu_j \, dn_d;$$

L^e_{photo} accounts for electron generation due to photoeffect,

$$L^e_{photo} = \int q_{photo} \, dn_d;$$

terms ν_e, ν_s, ν_c describe charging rates caused by recombination of electrons and ions on the dust particle surface. The value β_c is the conversion rate of primary ions into proton-hydrated ones. The ionization of a dust particle due to photoeffect is characterized by the rate q_{photo} and is determined by the solar radiation flux $F(\lambda)$ (see above).

The death of primary and proton-hydrate ions and electrons during charging due to their recombination on the surface of microparticles leads to a significant decrease in the concentration of the charged component of the ionosphere in the region of polar mesospheric clouds [9]. The calculation of microscopic currents of positive ions and electrons of the surrounding plasma on dust particles is carried out using the orbit-limited probe model [37. 38]. The interaction cross-sections of ions and electrons with a charged particle within the probe model are determined from the laws of conservation of energy and angular momentum. If dust particles are negatively charged, the probe approximation leads to the following expressions for charging rates:

$$\nu_e \approx \pi a^2 \left(\frac{8T_e}{\pi m_e}\right)^{1/2} n_e \exp\left(\frac{eq_d}{aT_e}\right),$$

$$\nu_i \approx \pi a^2 \left(\frac{8T_i}{\pi m_i}\right)^{1/2} n_i \left(1 - \frac{eq_d}{aT_i}\right)$$

For positively charged dust particles, the expressions for ν_e, ν_i take the form

$$\nu_e \approx \pi a^2 \left(\frac{8T_e}{\pi m_e}\right)^{1/2} n_e \left(1 + \frac{eq_d}{aT_e}\right)$$

$$\nu_i \approx \pi a^2 \left(\frac{8T_i}{\pi m_i}\right)^{1/2} n_i \exp\left(-\frac{eq_d}{aT_i}\right),$$

where T_e and T_i are the temperatures of electrons and ions, m_κ is the mass of a particle of type κ.

The model equations are written in the one-dimensional approximation (spatial coordinate is particle height h). The justification for such an approximation is related to the fact that the vertical size of mesospheric clouds (~1 km) is significantly smaller than the horizontal one (~10–100 km), and the horizontal transport velocities of dust particles are less than or of the order of vertical transport velocity, therefore we assume that at the considered times (hours, see [8, 9]) the horizontal displacement of particles can be neglected.

According to calculations within the framework of the model presented here, the characteristic sizes of dust particles in mesospheric clouds are $a \simeq 200$–250 nm. The corresponding charges of microparticles turn out to be $q_d \sim 50e$ in the presence of photoelectric effect and $q_d \sim -10e$ in its absence [9]. Note that the presence of a charge $|q_d| \sim 10e$ on a particle leads to a noticeable perturbation of the charged component of the ionospheric plasma, since the total charge of dust particles becomes comparable to the equilibrium total charges of electrons and ions.

The calculated parameters of dust particles, while matching the order of magnitude with experimental data, still slightly exceed the characteristic observed values ($a \simeq 100$ nm and $q_d \simeq -2e$ for the nighttime case, see [8,21]). This fact may be related to processes not accounted for in calculations based on the model described above. Among such processes, the Rayleigh-Taylor instability [39] appears important, which should naturally develop at the interface in the "gas + dust" system under gravity, in a situation where the upper half-space is occupied by dust and gas, while the lower one contains only gas [28, 40]. Dust clouds, as observed, have a sharp lower boundary, below which the concentration of dust particles becomes negligible compared to the particle concentration in the clouds. The mechanisms of formation of such a sharp boundary are associated with plasma-dust and some other physical processes, in particular, with the presence of air flows in the

ionosphere moving at a velocity of $v_{wind} \geqslant 0.1$ cm/s, as well as with the limited resources of water vapor (see [8–10]). Generally speaking, solutions within the hydrodynamic approach in describing plasma-dust systems that have sharp boundaries are quite typical (see, for example, [41]).

The dynamics of the boundary of the gas and dust system, unlimited in the horizontal direction, in this case is described by the Euler and continuity equations, the linearization of which in studying the stability of the stationary solution leads to the dispersion equation

$$\tilde{\gamma}^3 + \tilde{\gamma}^2\left[\alpha\left(1+\frac{n_d m}{2\rho}\right)+\frac{|\mathbf{k}|g}{\alpha}\right]+$$
$$+\tilde{\gamma}|\mathbf{k}|g-\frac{n_d m|\mathbf{k}|g\alpha}{2\rho}=0. \qquad (13)$$

Here $|k|$ is the wave number, $\tilde{\gamma}$ is the instability increment, n_d is the concentration of dust particles,

$$\alpha = 2\sqrt{\frac{2}{\rho}}\frac{Gn_{H_2O}T}{r_d v^{th}_{H_2O} a},$$

where G is a coefficient of the order unity, determined by the peculiarities of neutral interaction with the particle surface. For example, $G = 1$ in the case of complete absorption or specular reflection of neutrals from the particle surface during collision and $G = 1 + \rho/8$ in the case of complete accommodation [15]. The dispersion equation (13) is obtained under the condition of sufficiently small electric fields and is valid, including when $|E| \sim 1$ B/m, which, as can be expected [8], is fulfilled under Earth's ionospheric conditions.

4. RESULTS

The system of equations (3)–(12) allows determining the altitude distribution of particles comprising noctilucent clouds. Figure 2 illustrates such distribution. The initial size of cloud dust particles is 10 nm. Upon entering the condensation zone, dust particles begin to increase in size due to desublimation of H_2O vapors. The upper layers, initially located at the boundary between zones with supersaturated and unsaturated vapors, evolve more slowly than the layers initially located directly in the condensation zone. At a certain point in time, particles reach characteristic sizes of $\simeq 0.2$–0.3 μm.

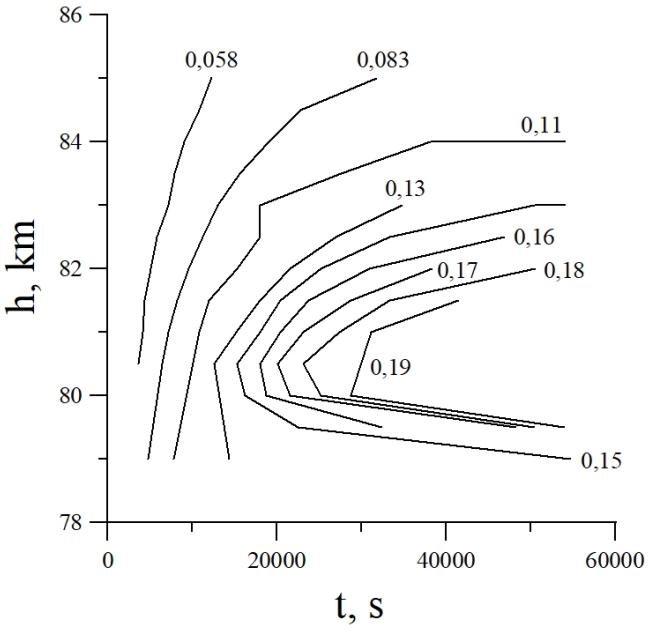

Fig. 2. Time dependence of the vertical distribution of dust particles in polar mesospheric clouds, forming due to sedimentation of a dust cloud of nuclei, initially comprising a model concentration profile with an initial dust particle size of 10 nm. Upon entering the condensation zone, dust particles begin to increase in size due to desublimation of vapors H_2O, forming a layer of particles with a characteristic size of $\simeq 0.2$–0.3 μm at altitudes of about 80 km. Numbers above the curves indicate particle sizes in micrometers

The characteristic sedimentation time of the dust cloud is on the order of hours/tens of hours.

As noted above, the results obtained according to (3)–(12) exceed the observed data by approximately 2–3 times, therefore it is necessary to separately account for factors not considered in the system (3)–(12). In particular, one such factor is the development of Rayleigh–Taylor instability at the lower cloud boundary. As numerical analysis shows, the dispersion equation (13), at temperature and neutral concentration values typical for the ionosphere, has three real roots, two of which are negative and one positive. For instability development, the positive root corresponding to the growing mode is of interest.

Figure 3 shows the dependence $\tilde{\gamma}(k)$ for different values of dust particle sizes and concentrations. Ionosphere parameters correspond to an altitude of $h = 85$ km, for which $T = 129.5$ K, $\rho = 8.22 \cdot 10^{-6}$ kg/m^3. The value $\tilde{\gamma}(k)$, as seen from the figure, increases with the growth of dust parameters. Furthermore, it is evident that asymptotically $\tilde{\gamma}(k)$ quickly reaches a stationary

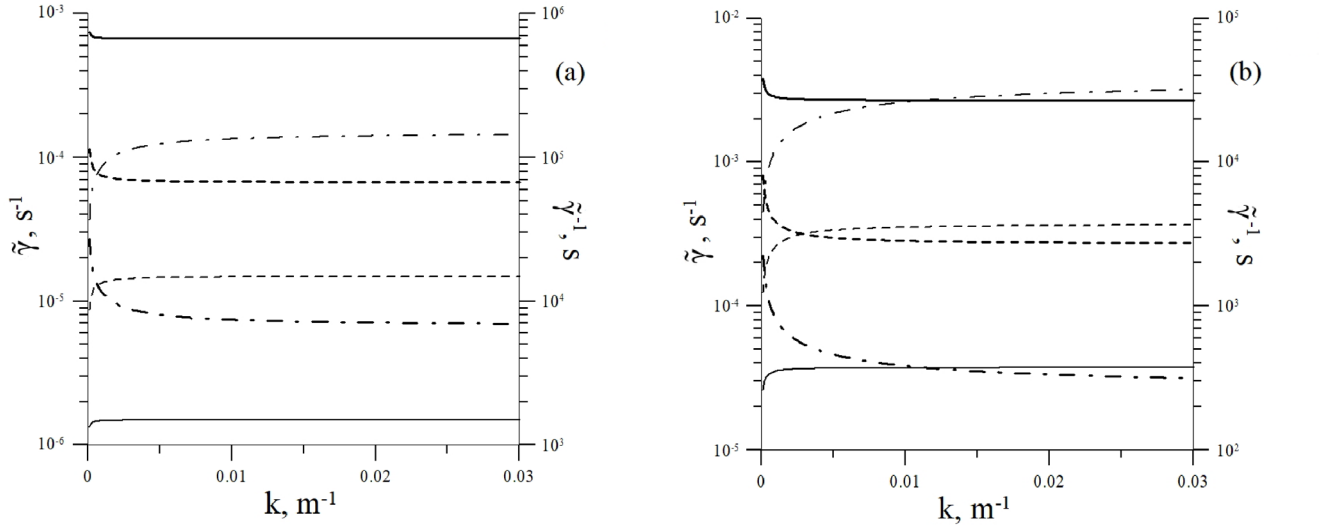

Fig. 3. Dependencies of the Rayleigh–Taylor instability growth rate $\tilde{\gamma}$ (thin lines) and value $\tilde{\gamma}^{-1}$ (bold lines) on the wave number $|k|$ for $h = 85$ km. Solid curves correspond to $n_d = 10$ cm^{-3}, dashed $n_d = 100$ cm^{-3}, dash-dotted $n_d = 1000$ cm^{-3}. Panel (*a*)corresponds to dust particle size $a = 20$ nm, (*b*) — to dust particle size $a = 100$ nm

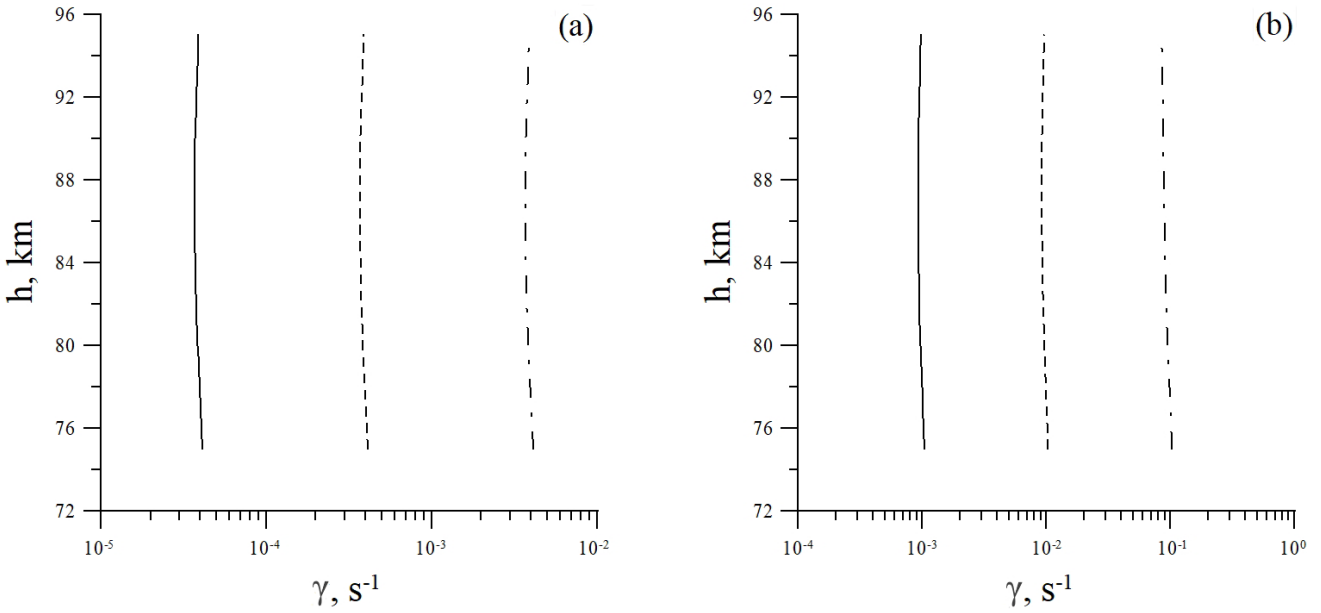

Fig. 4. Dependencies of the maximum Rayleigh–Taylor instability growth rate g on height h for dust particle concentrations $n_d = 10$ cm^{-3} cm (solid curves), $n_d = 100$ cm^{-3} (dashed curves), $n_d = 1000$ cm^{-3} (dash-dotted curves). Panel (*a*) corresponds to dust particle size $a = 20$ nm, (*b*) — to dust particle size $a = 500$ nm.

value g, which determines the characteristic time of instability development, coinciding in order with the value g^{-1}. Note also that $\mathsf{g} \sim n_d$ and $\mathsf{g} \sim a^2$.

Thus, the instability increment $\tilde{\gamma}$, starting from a certain value $|\mathbf{k}|$, reaches a maximum g. Figure 4 shows altitude profiles of the maximum increment dependence g for various concentrations and sizes of dust particles. The value g increases with the growth of dust parameters and, therefore, should limit the size of dust cloud microparticles from above.

Fig. 5 shows graphs of the dependence of the characteristic time of Rayleigh–Taylor instability development $\mathsf{t} = \mathsf{g}^{-1}$ on the dust particle size of the cloud compared to the characteristic sedimentation

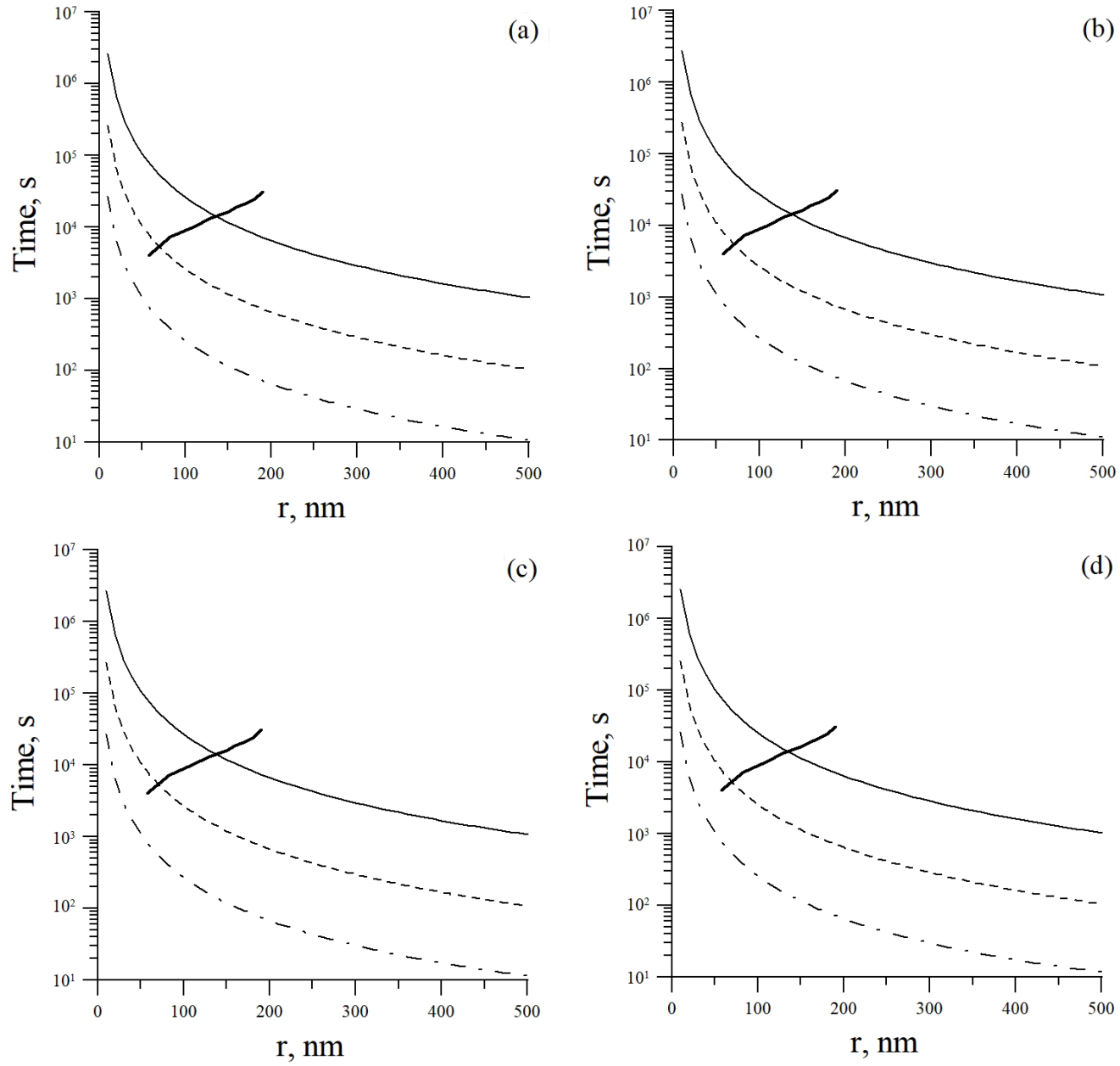

Fig. 5. Dependencies of the characteristic time of Rayleigh–Taylor instability development and sedimentation time of dust particles on their sizes. Calculation results are presented for heights 80 (*a*), 85 (*b*), 90 (*c*), 95 (*d*) km. Thin solid curves correspond to dust particle concentrations $n_d = 10$ cm^{-3}, dashed — $n_d = 100$ cm^{-3}, dash-dotted — $n_d = 1000$ cm^{-3}. Dependencies of dust particle sedimentation time are represented by thick solid lines

time for altitudes 80, 85, 90 and 95 km. Typical atmospheric parameter values at these altitudes are respectively (see [42]):

at $h = 80$ km — $T = 141.3$ K, $\rho = 1.85 \times 10^{-5}$ kg/m^3;

at $h = 85$ km — $T = 129.5$ K, $\rho = 8.22 \times 10^{-6}$ kg/m^3;

at $h = 90$ km — $T = 130.0$ K, $\rho = 3.42 \times 10^{-6}$ кг/m^3;

at $h = 95$ km — $T = 143.2$ K, $\rho = 1.41 \times 10^{-6}$ kg/m^3.

In Fig. 5, it can be seen that the sedimentation time does not exceed $\tau = \gamma^{-1}$ only at sufficiently small dust particle sizes. Thus, even at low concentrations $n_d = 10$ cm^{-3} the sedimentation time equals $\tau = \gamma^{-1}$ already at $a_{\text{„}}$ 150 nm, thereby limiting the size of cloud microparticles, as at larger sizes the process of layered structure destruction due to instability development becomes more effective than its formation due to water vapor condensation.

For typical ionospheric values $n_d = 100$ cm^{-3} the upper boundary and turns out to be even smaller.

Note that for this work, it is not the fact of cloud destruction that is important, but that in the case of Rayleigh–Taylor instability development, this destruction occurs when cloud microparticles reach a certain threshold size. The action of instability thus substantiates the fundamental impossibility of the existence of large particle clouds, which corresponds to observational data.

5. CONCLUSION

Thus, the equations of the model describing plasma-dust structures in the Earth's ionosphere in a self-consistent manner are presented. It is shown that, unlike the Martian ionosphere, on Earth there is a reduced influence of such factors as dust particle deceleration due to condensate molecule adhesion (analog of reactive force) and decrease in Knudsen viscous friction force in the condensation zone. At the same time, the dynamics of the charged component of the ionosphere on Earth turns out to be more complex than on Mars.

Based on the presented equations, it is shown that the characteristic particle size of the cloud predicted by the model exceeds the observed values by approximately 2–3 times. It turns out that an important factor affecting the formation of plasma-dust clouds that should be taken into account is the Rayleigh-Taylor instability, which leads to the fact that plasma-dust clouds can exist only at sufficiently small sizes of their constituent dust particles.

REFERENCES

1. S.I. Popel, Priroda 9, 15 (2015).

2. S.I. Popel, S.I. Kopnin, I.N. Kosarev, M.Y. Yu, Adv. in Space Res. 37, 414 (2006).

3. Yu.N. Izvekova, Yu.S. Reznichenko, S.I. Popel, Plasma Phys. Rep. 46, 1205 (2020).

4. V.E. Fortov, Yu.M. Baturin, G.O. Morfill, O.F. Petrov, Plasma Crystal, Space Experiments, Moscow: Fizmatlit (2015) [in Russian].

5. S.I. Popel, A.P. Golub', A.I. Kassem, L.M. Zelenyi, Phys. Plasmas 29, 013701 (2022).

6. S.I. Popel, L.M. Zelenyi, A.P. Golub', A.Yu. Dubinskii, Planetary and Space Science 156, 71 (2018).

7. S.I. Popel, A.A. Gisko, Nonlin. Processes Geophys. 13, 223 (2006).

8. B.A. Klumov, S.I. Popel, R. Bingham, JETP Lett. 72, 524 (2000).

9. B.A. Klumov, G.E. Morfill, S.I. Popel, JETP 100, 152 (2005).

10. A.Yu. Dubinskii, S.I. Popel, JETP Lett. 96, 21 (2012).

11. S I Popel, S I Kopnin, M Y Yu et all, J. Phys. D: Appl. Phys. 44, 174036 (2011).

12. V.E. Fortov, A.V. Ivlev, S.A. Khrapak et all, Phys. Reports. 421, 1 (2005).

13. P.K. Shukla, A.A. Mamun, Introduction to Dusty Plasmas Physics, Bristol/Philadelphia: Inst. Phys. Publ. (2002).

14. V.N. Tsytovich, Physics-Uspekhi 40, 53 (1997).

15. V.E. Fortov, A.G. Khrapak, S.A. Khrapak et all, Physics-Uspekhi 47, 447 (2004).

16. V.N. Tsytovich, G.E. Morfill, S.V. Vladimirov, H.M. Thomas, Elementary Physics of Complex Plasmas, Berlin: Springer (2008).

17. U. von Zahn, G. Baumgarten, U. Berger et all, Atmos. Chem. Phys. 4, 2449 (2004).

18. J.Y.N. Cho, J.Röttger, J. Geophys. Res. 102, 2001 (1997).

19. M. Gadsden, W. Schröder, Noctilucent Clouds, Berlin: Springer-Verlag (1989).

20. H. Thomas, G.E. Morfill, Nature 379, 806 (1996).

21. F. Montmessin, J.-L. Bertaux, E. Quémerais et all, Icarus 183, 403 (2006).

22. https://www.newsru.com/hitech/30may2021/mars_clouds.html

23. F. Montmessin, B. Gondet, J. P. Bibring et all, J. Geophys. Res. 112, E11S90 (2007).

24. J. A. Whiteway, L. Komguem, C. Dickinson et all, Science 325, 68 (2009).

25. P.O. Hayne, D.A. Paige, J.T. Schofield et all, J. Geophys. Res. 117, E08014 (2012).

26. A.Yu. Dubinskii, Yu.S. Reznichenko, S.I. Popel, Plasma Phys. Rep. 45, 928 (2019).

27. Yu.S. Reznichenko, A.Yu. Dubinskii, S.I. Popel, J. Phys.: Conf. Ser. 1556, 012072 (2020).

28. Yu.S. Reznichenko, A.Yu. Dubinskii, S.I. Popel, JETP Lett. 117, 428 (2023).

29. R.P. Turco, O.B. Toon, R.C. Whitten et all, Planet. Space Sci. 30, 1147 (1982).

30. R. A. Goldberg, R. F. Pfaff, R. H. Holzworth et all, Geophys. Res. Lett. 28, 1407 (2001).

31. M. A. Leontovich, Introduction to Thermodynamics, Moscow: Gos. Izdat. Tekh.-Teor. Liter., p. 158 (1952) [in Russian].

32. G.C., Reid, J. Atmos. Sci. 32, 523 (1975).

33. E. Kopp, Adv. Space Res. 25, 173 (2000).

34. A.V. Pavlov, Surveys in Geophysics 35, 259 (2014).

35. A. V. Filippov, I. N. Derbenev, N. A. Dyatko et all, JETP 125, 246 (2017).

36. A.Yu. Dubinsky, Yu.S. Reznichenko, S.I. Popel, Sol. Syst. Res. 57, 214 (2023).

37. F.F. Chen, in Plasma Diagnostic Techniques, ed. by R.H. Huddlestone and S.L. Leonard, Academic, New York (1965), Chap. 4.

38. M.S. Barnes, J.H. Keller, J.C. Forster et all, Phys. Rev. Lett. 68, 313 (1992).

39. C. Völtz, W. Pesch, I. Rehberg, Phys. Rev. E. 65, 011404 (2001).

40. R.S. Savel'ev, N.N. Rozanov, G.B. Sochilin, S.A. Chivilikhin, Nauchno-Tekh. Vestn. S.-Peterb. Gos. Univ. Inf. Tekhnol., Mekh. Opt. 73, 18 (2011).

41. V.N. Tsytovich, Physics-Uspekhi 58, 150 (2015).

42. Standard atmosphere. Parameters, GOST 4401-81, Moscow: IPK Izdatelstvo standartov (2004) [in Russian].